

Spiral-Phase-Defect Resonator and Its Application in Vortex Laser of Controllable Topological Charges

Yuan-Yao Lin  and Yu-Wei Li

Abstract—An optical resonator with a spiral-phase defect is proposed for vortex laser generation. Theoretical models and calculations were conducted to predict the topological charge distribution of the emitted vortex laser. Utilizing a reflective spatial light modulator that creates a spiral-phase defect of variable radius and azimuthal phase modulation, vortex beams with controllable topological charges and intensity distributions were demonstrated experimentally.

Index Terms—Optical vortex, digital lasers, spiral-phase-defect resonator.

I. INTRODUCTION

RECENTLY, researchers have paid great attention to coherent radiation with structured phase patterns [1], [2]. Coherent radiation carrying orbital angular momentum (OAM) is particularly appealing because of its applicability in high-capacity optical communication systems with OAM multiplexing [3], superresolution microscopy with vortex stimulated emission depletion technique [4] and optical trapping of micro-sized or nano-sized particles [5]. Advanced particle manipulation was realized using vortex array generated by the interference of Airy beams [6], [7]. Laser ablation using vortex laser for pillar structure fabrication [8] were demonstrated in industry. In scientific researches, orthogonal OAM states were proposed as foundations to build high-dimensional quantum communication link that could potentially improve photon efficiency [9]. This demand for easy access to lasers carrying OAMs is increasing, which accelerates the development of vortex laser technologies. Passive mode conversion techniques, such as diffractive optics [10], spatial light modulators [11], [12], and engineered anisotropic materials [13], are mature and have very high conversion efficiencies of more than 90% [14]. Their limited working range, less desirable beam quality, and OAM purity limit the usefulness of structured light in long-range OAM multiplexing communications [15]. In contrast, direct emission of coherent light carrying OAM from laser resonators is more desirable for practical use because the radiation mode is better discriminated and filtered by the laser cavity [16].

Manuscript received 1 June 2022; revised 2 August 2022; accepted 17 August 2022. Date of publication 22 August 2022; date of current version 1 September 2022. This work was supported by the Ministry of Science and Technology of Taiwan under Grant MOST-110-2112-M-110-012. (Corresponding author: Yuan-Yao Lin.)

The authors are with the Department of Photonics, National Sun Yat-sen University, Kaohsiung City 80424, Taiwan (e-mail: yuyalin@mail.nsysu.edu.tw; perry851228@gmail.com).

Digital Object Identifier 10.1109/JPHOT.2022.3200490

In 1999, Oron et al. pioneered direct vortex lasing with an intracavity spiral-phase element at a wavelength of 10.6 μm [17], [18]. In 2010, Ito et al. generated hollow scalar and vector beams in a solid-state laser resonator with a spot-defect mirror [19]. In 2012, Kano and coworkers used a He–Ne laser cavity with a spot-defect mirror to generate a vortex beam of very high purity, which surpassed any passive conversion scheme at that time [20]. The approach of Ito et al. provided a doughnut-shaped net gain region to excite the vortex beam selectively when it experienced a higher gain than the fundamental mode in the laser cavity. Therefore, it is equivalent to Chen and Lan’s proposal in 2001. They shaped the pump beam into a doughnut-like profile to excite the Laguerre Gaussian (LG) family of $TEM_{0,l}^*$ and $TEM_{0,l}$ modes [21]. However, in a laser resonator with cylindrical symmetry, the degeneracies in the LG $TEM_{0,l}^*$, $TEM_{0,-l}^*$, and $TEM_{0,l}$ (the coherent superposition of LG $TEM_{0,l}^*$ and $TEM_{0,-l}^*$ modes) modes also induce laser instability, self-modulation, and even chaos [21]. In 2014, Lin et al. invented an intracavity mode selection element that overcame the degeneracy and discriminated $TEM_{0,l}^*$ and $TEM_{0,-l}^*$. It demonstrated complete control of the handedness of directly excited LG modes in a solid-state laser adopting a doughnut-shaped pump scheme [22] and inspired later research on vortex generation with an intracavity low-finesse Fabry–Perot etalon [23]. Moreover, direct vortex lasing was possible by composite cavities resonating the fundamental and higher-order modes using an interferometric output coupler [24]. Replacing the spiral-phase element with a pair of Q-plates, higher-order Poincaré sphere beams were generated from a laser resonator [25]. The laser resonator designs for direct vortex emission are azimuthally symmetrical [17], [18], [19], [20], [21], [22], [23], [24], [25].

In 2018, an azimuthal symmetry breaking (ASB) laser resonator with a hemispherical configuration was proposed. It rejects the resonance of on-axis modes, such as the LG family. An optical vortex laser formed by the coherent superposition of off-axis multiple-pass transverse modes that are mutually nonorthogonal was demonstrated, and a vortex purity greater than 99.99% was achieved in a continuous-wave regime [26]. Laser beams with controllable OAM are important tools for the development of OAM-related science and technology. In particular, real-time laser pattern tuning without alternating optics has been introduced using a digital laser, which includes an intracavity spatial light modulator (SLM) to manipulate the amplitudes and phases of the intracavity field [27]. Laser beams with on-demand lateral field distributions are generated

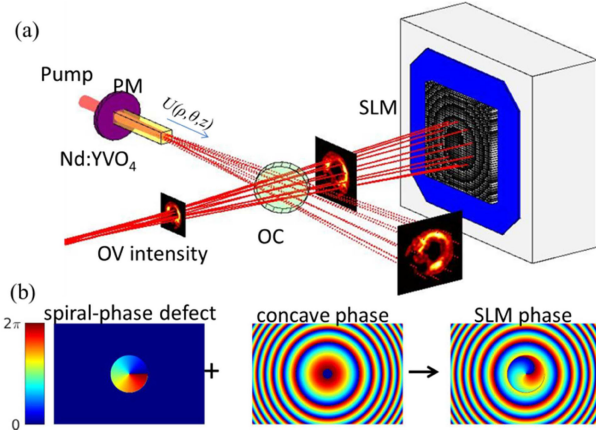


Fig. 1. (a) Schematic diagrams of the laser formed by a pump mirror (PM) and the reflective-type SLM. The output coupler (OC) reflects small resonating power stimulated and amplified by Nd:YVO₄ laser crystal at a wavelength of 1064 nm. (b) Phase modulation provided by the SLM, which combines finite-sized spiral phase and concave phase.

from digital lasers with a phase-only SLM [28]. Although the vortex beam can be generated in a digital laser with amplitude modulation, similar to the concept of a laser cavity with a spot-defect mirror [19], the control over the sign and quantity of the topological charge is not quite convenient without broken azimuthal symmetry. To obtain better control over the topological charge of a direct-emitted vortex laser, a laser resonator containing an on-axis defect, which is introduced by a spiral-phase element with a topological charge and a finite radius, is proposed [29]. The parameter space for generating a vortex beam with different topological charges was obtained theoretically, and the vortex lasers were demonstrated experimentally in a digital laser system at a wavelength of 1064 nm with controllable topological charge. This work not only provides an efficient and convenient approach to generate optical vortices but also extends the capability of digital laser platforms.

II. MODAL ANALYSIS OF SPIRAL-PHASE DEFECT CAVITY

The proposed laser resonator is illustrated in Fig. 1(a). It was formed by a reflective-phase-only SLM and a flat pump mirror. A polarization selective gain medium, Nd:YVO₄, is placed near the pump mirror and a dichroic mirror is placed in the front of the SLM, which functioned as an output coupler for the resonating field and a separator for the residue pump. The SLM is encoded to modulate the phase of the incoming electromagnetic field. As illustrated in Fig. 1(b), the modulation includes a concave phase that supports stable resonance and an on-axis finite-sized spiral phase, which serves as a defect.

The cylindrical symmetry, except the azimuthal symmetry breaking at the central region of the defect, makes possible the expansion of the radiation pattern in terms of a coherent superposition of the orthogonal basis of LG modes supported by the cavity without the intracavity singular defect. Here, θ , z are the azimuthal and spatial coordinates, respectively, and $\rho = \sqrt{2}r/W(z)$ is the radial coordinate scaled to the beam radius of the cavity mode. The electromagnetic field resonating

in the cavity can be written as

$$U(\rho, \theta, z) = \sum_{p, l} A_{p, l} LG_p^l(\rho, \theta, z) \quad (1)$$

where $A_{p, l} = \frac{W(z)^2}{2} \int_0^\infty \rho d\rho \int_0^{2\pi} d\theta U(\rho, \theta, z) LG_p^{l*}(\rho, \theta, z)$ is the coefficient of the LG basis function $LG_p^l(\rho, \theta, z)$ of radial index p and azimuthal index l in the cavity [1]. When a particular field component $LG_p^l(\rho, \theta, z)$ resonating in the cavity is reflected by the SLM, its phase is modulated and consequently is lead to modal losses and intermodal coherent scatterings, which can be estimated by the computed matrix element.

$$\begin{aligned} \sigma_{p', l}^{l', l} &= e^{i\Delta\phi} \int_0^\infty \rho d\rho \int_0^{2\pi} d\theta LG_{p'}^{l'*}(\rho, \theta, z) \\ &R_{SLM} LG_p^l(\rho, \theta, z) \\ &= e^{i\Delta\phi} \int_0^{\rho_{SPD}} d\rho \rho^{|l|+|l'+1|} L_p^{|l|}(\rho^2) L_{p'}^{|l'|}(\rho^2) e^{-\rho^2} \\ &\delta(l' - l + q) + e^{i\Delta\phi} \int_{\rho_{SPD}}^\infty d\rho \int_0^{\rho_{SPD}} d\rho \rho^{|l|+|l'+1|} L_p^{|l|}(\rho^2) \\ &L_{p'}^{|l'|}(\rho^2) e^{-\rho^2} \delta(l' - l) \end{aligned} \quad (2)$$

Here, $L_p^{|l|}$ is the Laguerre polynomial, and the phase function is given by

$$\begin{cases} R_{SLM} = 1, & \rho > \rho_{SPD} \\ R_{SLM} = \exp[iq\theta], & \rho \leq \rho_{SPD} \end{cases}$$

where ρ_{SPD} is the radius of the spiral-phase defect (SPD), and q is its topological charge. $\Delta\phi$ is phase difference from Guoy phase given by, $\Delta\phi = (|l| + 2p - |l'| - 2p') \tan^{-1}(\frac{z_{SPD}}{z_R})$ in which z_{SPD} is the distance between the SPD and the location of waist of radius of laser in the cavity. z_R is the Rayleigh range of the laser beam. The nonvanishing matrix element $\sigma_{p', p}^{l'+q, l}$ indicates coupling from the $LG_p^l(\rho, \theta, z)$ mode to the $LG_{p'}^{l'+q}(\rho, \theta, z)$ mode. Additional modal losses are introduced when $\sigma_{p', p}^{l', l} < 1$ significantly decreases with a large ρ_{SPD} . Although $\sigma_{p', p}^{l', l}$ and $\sigma_{p', p}^{l'+q, l}$ make coupling between modes of different radial indices possible, this discussion is restricted to those modes ($p = 0$) that acquire a higher gain portion under a pump beam with a finite beam radius. An analytical expression for the matrix element of zero radial index writes

$$\begin{aligned} \sigma_{0, 0}^{l', l-q} &= -\sqrt{\frac{4}{(|l'|!) (|l' - q|)!}} \frac{\rho_{SPD}^{\frac{l_1}{2}}}{\pi(-1)^{\frac{l_1}{4}} (l_1 + 2)} e^{-\frac{\rho_{SPD}^2}{2}} \\ &\times M_{-\frac{l_1}{4}, \frac{l_1}{4} + \frac{1}{2}}(-\rho_{SPD}^2) e^{i\Delta\phi} \end{aligned} \quad (3)$$

$$\begin{aligned} \sigma_{0, 0}^{l', l} &= -\frac{2}{(|l'|)!} \left[\frac{\Gamma(\frac{l_2}{2} + 1)}{2} + \frac{\rho_{SPD}^{\frac{l_2}{2}}}{(-1)^{\frac{l_2}{4}} (l_2 + 2)} e^{-\frac{\rho_{SPD}^2}{2}} \right. \\ &\left. \times M_{-\frac{l_2}{4}, \frac{l_2}{4} + \frac{1}{2}}(-\rho_{SPD}^2) \right] \end{aligned} \quad (4)$$

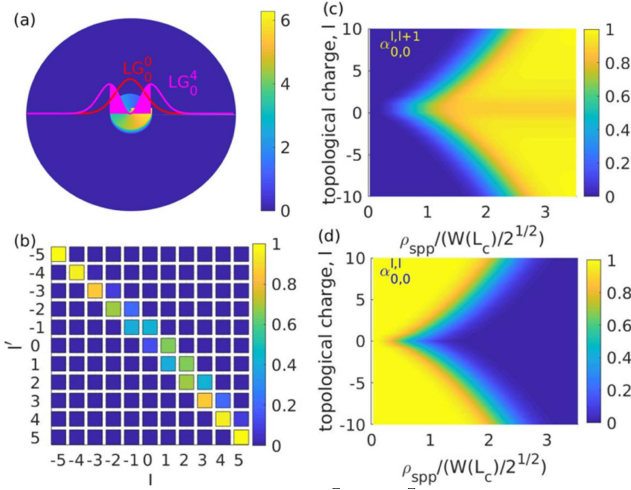


Fig. 2. (a) Radial field distribution of LG_0^0 and LG_0^4 modes and a SPD of radius equal to $W(L_c)/2$. The filled area of LG_0^0 mode presents the magnitude of scattering coefficient and the unfilled area corresponds to the magnitude of reflection coefficient. (b) shows the magnitude of matrix element presented in colors from LG_0^l mode to $LG_0^{l'}$ mode given $\sqrt{2}\rho_{SPD}/W(L_c) = 1$. (c) The scattering coefficient and (d) the reflection coefficient of LG_0^l mode reflected by a SPD.

where $l_1 = |l| + |l - q|$, $l_2 = 2|l|$, $\Gamma(x)$ is the gamma function, and $M_{a,b}(x)$ is the Whittaker M function [30].

When a spiral phase element is placed inside a laser cavity, it is likely to ladder up the OAM carried by the resonating field and the lasing is forbidden. It is very critical in vortex generation in a laser cavity with azimuthal symmetry breaking. To overcome the difficulty, a cylindrical focusing lens was required in Oron's proposal in 1999 and 2000 [17], [18], which restored the broken azimuthal symmetry and swapped back the topological charges. Moreover, a laser cavity with intracavity spiral phase element resonating only off-axis modes was introduced to overcome the singularity [26], [32]. In a SPD of finite radius encoded by SLM, the broken azimuthal symmetry was introduced into the laser cavity as well. Upon the incidence of the SLM, the wavefront of a paraxial beam is partly modulated only within the region where spiral phase was encoded which is illustrated in Fig. 2(a). The modulated beam thus presents different topological charges inside and outside the spiral phase region. It is in analogy to a coherent scattering process and can be quantified by projecting the modulated field onto an orthogonal basis, say Laguerre Gaussian beams of cylindrical symmetry that are supported by the resonator. The scattering efficiency upon the incidence of the SPD from one mode to another can be calculated by the matrix element by (2). When the size of SPD is larger, more field experiences wavefront modulation upon incidence to SPD. Stronger scattering occurs and the field remaining its modal property before incidence thus is less. For example, a field at its transient state of LG_0^l can be coupled to some other mode LG_0^{l+1} by the coherent scattering process quantified by the coefficient $\sigma_{0,0}^{l+1,l}$ when it is reflected by the SPD in which the finite-sized spiral phase has a topological charge of 1. Notably scattering to a mode of azimuthal index different from $l+1$ is impossible due to the angular momentum conservation law. The

coefficient $\sigma_{0,0}^{l,l}$ describes the portion of field amplitude remain in the LG_0^l state. Moreover, LG_0^l state also receives the field scattered from LG_0^{l-1} mode quantified by the coefficient $\sigma_{0,0}^{l,l-1}$. In general, the modulus of $\sigma_{0,0}^{l+1,l}$ is less than 1 and it infers that part of field in the state LG_0^l is lost upon the reflection on SPD. Regarding to the scattering coefficient $\sigma_{0,0}^{l+1,l}$ and reflection coefficient $\sigma_{0,0}^{l,l}$ of a SPD with a topological charge of 1, it is shown in the Fig. 2(c) and (d) that the modulus of the scattering coefficient $\sigma_{0,0}^{l+1,l}$ and reflection coefficient $\sigma_{0,0}^{l,l}$ as a function of the topological charge l and defect radius ρ_{spp} . It is very clear that increasing the defect radius causes the scattering coefficient increasing and the reflection coefficient decreasing. Because the intensity distribution of a mode of higher azimuthal indices are less overlapped with the SPD region as shown in Fig. 2(a), a LG Gaussian beam of higher azimuthal indices experiences less scattering and more reflection. The magnitude of matrix element resented in colors were illustrated in Fig. 2(b) showing the coherent scattering from LG_0^l mode to $LG_0^{l'}$ mode given that $\sqrt{2}\rho_{SPD}/W(L_c) = 1$. The diagonal elements stand for the reflection coefficients $\sigma_{0,0}^{l,l}$ and the upper diagonal ones stand for the scattering coefficients $\sigma_{0,0}^{l+1,l}$.

A particular mode can extract the most of the power from the pump under the dynamical balance of modal loss due to the scattering from SPD, intermodal coupling from a mode obeying azimuthally phase matching (angular momentum conservation) and modal gains. It consequently determines the laser output mode. Therefore the SPD of a finite radius plays a crucial role in stably manipulating the sign and magnitude of the OAM of the laser output and prevents the ladder function for OAM. Nevertheless, for a SPD of infinite radius (a radius much greater than the beam radius of lasers), the magnitude of scattering coefficient approaches one, the ladder function for OAM in the cavity is dominant and the lasing is not possible.

The multiple transverse mode oscillation dynamics can then be described by coupled laser rate equations for the upper-level population n_u , Fourier component of modal population n_l , and modal photon flux density s_l [31], [32],

$$\frac{dn_u}{dt} = W_{\text{pump}} - \frac{n_u}{\tau_2} - \sum_i C_i \left(n_u - \frac{n_i}{2} \right) s_i c \sigma \quad (5)$$

$$\frac{dn_l}{dt} = C_l n_u s_l c \sigma - n_l \left(\gamma_{21} + \sum_i C_i s_i c \sigma \right) \quad (6)$$

$$\frac{ds_l}{dt} = \frac{s_l}{t_r} \left[2C_l \left(n_u - \frac{n_l}{2} \right) \sigma l_g - \ln \left(\frac{1}{R_{pm} R_0} \right) \right] + \left(\sigma_{0,0}^{l,l-q} \right)^2 s_{l-q} - 2 \ln \left(1 - \sigma_{0,0}^{l,l} \right) \quad (7)$$

The gain cross section, $\sigma = 2.35 \times 10^{-19} \text{ cm}^2$, crystal length, $l_g = 0.8 \text{ cm}$, spontaneous emission rate, $\gamma_{21} = 2000 \text{ s}^{-1}$, and upper-level lifetime, $\tau_2 = 210 \text{ } \mu\text{s}$, are used for the Nd:YVO₄ laser crystal [31]. The cavity round trip time, $t_r = 1 \text{ ns}$, pump mirror reflectivity, $R_{pm} > 0.999$, and intrinsic power reflectance of liquid-crystal-on-silicon SLM (Sentec SLM-300), $R_0 = 0.8$, are adopted. Moreover, the population at a lower level of atomic

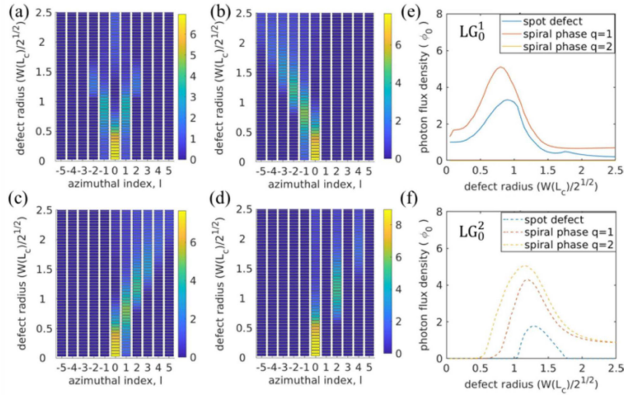


Fig. 3. Calculated steady-state photon flux density of LG_0^l mode with varying radii of defect regions carrying (a) losses, (b) topological charge of -1 , (c) topological charge of $+1$, and (d) topological charge of $+2$. Particular resonating components (e) LG_0^1 and (f) LG_0^2 are plotted using different defect types of varying radii.

transition is assumed to be negligible. The gain fractions C_i are computed by the overlap integral of the pump beam and resonating cavity mode in the gain crystal. The pump diode laser at 808 nm provides a pump speed of W_{pump} and is focused on the laser cavity, yielding a beam radius of $200 \mu\text{m}$ and M^2 value of 100. The SLM emulating a concave mirror with a radius of curvature of 20 cm was separated by a distance of 15 cm, as illustrated in Fig. 1(a). The OC placed in the cavity reflects a small resonating power ($<0.6\%$) stimulated and amplified by the Nd:YVO₄ laser crystal at a wavelength of 1064 nm. Without an SPD, the laser beam radius is $184 \mu\text{m}$ in the laser crystal and $332 \mu\text{m}$ on the SLM panel.

Equations (3)–(7) make it possible to predict multiple-mode lasing dynamics by direct integration using fourth-order Runge–Kutta algorithm. While maintaining a constant pump rate well above the threshold, the multimode laser system reaches a steady state within a few microseconds. The steady-state azimuthal modal distribution is evaluated for a resonator with an SPD of various radii scaled to the beam radius of the cavity mode and of different topological charges. For comparison, Fig. 2(a) shows the calculated steady-state photon flux density when the defect is purely absorptive. As the defect radii increase, the resonating mode of a large magnitude in topological charges dominates. Degeneracy is observed because the positive and negative topological charges cannot be discriminated. With SPD, the degeneracy breaks, as shown in Fig. 2(b) and (c), in which the SPD carries topological charges of -1 and $+1$, respectively, the sign of the topological charge of the resonating vortex mode can be selected, and the magnitude of the topological charge of the vortex mode increases with the defect radius. The topological charge of the resonating mode hops at a pace equal to the topological charge of the SPD, as illustrated in Fig. 2(c) and (d). The SPD is more efficient in generating vortex light than an absorptive spot defect similar to Ito’s proposal [19]. As shown in Fig. 2(e), the excitation of LG_0^1 requires a smaller SPD radius than the spot defect radius, and a higher photon flux density is generated. Moreover, to excite a mode of large

topological charge in magnitude (for example, the LG_0^2 mode), direct coupling introduced by an SPD of high topological charge ($q = 2$) significantly enhances the generation of photon flux density in the cavity. This means that direct coupling by the SPD of desirable topological charge is more effective than cascaded coupling by an SPD carrying the its fractions, not to mention any mode-matching method in the spot-defect cavity [19]. Notably the modal distribution in the proposed spiral-phase-defect resonator can be considered resonant holography [33]. The multiple round pass diffractive process makes topological charge of the laser beam function of both topological charge q and radius ρ_{spd} of the SPD. In contrast, vortex beam generated by a single pass diffractive optics reveals only the azimuthal Fourier components of the phase pattern [12].

III. EXPERIMENTS AND DISCUSSION

A diode-pumped solid-state laser system following the setup photographed in Fig. 4(a) was built to demonstrate vortex lasing in an SPD resonator. The SLM was encoded to pattern an SPD of a finite radius on the cavity axis in addition to a quadratic phase serving as a concave mirror with a 20-cm radius of curvature. First a wrapped concave phase of the form $[k \frac{r^2}{R}]_{r>0}$ is implemented shown in Fig. 1(b) where r is the spatial coordinate centered at the cavity axis and k is the wave vector. It serves as a concave cavity mirror of a radius of curvature $R = 20$ cm without azimuthal modulation of the SPD. Then SPD of the phase distribution $l\theta$ given $r < R_{\text{SPD}}$ where l is the topological charge and R_{SPD} is the radius of the SPD shown Fig. 1(b). The overall phase function implemented by SLM phase writes, $[k \frac{r^2}{R}]_{r>0} + [l\theta]_{r<R_{\text{SPD}}}$. It is wrapped to 2π , discretized into 256 gray levels in magnitude and addressed spatially into the 1920×1200 pixels of the SLM panel with a pixel pitch of $8 \mu\text{m}$. A 9-mm-long a-cut Nd:YVO₄ crystal was placed to provide optical gain to parallel polarized light (with respect to the surface of the optical table), which responds to the phase modulation of the SLM. In our design illustrated in Fig. 4(a), a dichroid mirror (DM) with antireflection coating at 1064 nm and high reflection coating at 808 nm is placed to remove the residue power from 808 nm pump laser to hit the SLM behind. At the same time, this dichroid mirror reflects 0.6% of the oscillating electromagnetic field at 1064 nm also served as the output coupler. When the vortex beam lased above the threshold, output power of nearly 1 mW was measured by power detector and the intracavity laser power was estimated to be 167 mW. According to the specification of the high power SLM (Santec SLM-300), which sustains optical power of 200W over the 1.5 cm^2 panel in continuous operation, the maximum power in the resonator should be less than 0.23W when the beam radius on SLM was calculated to be $332 \mu\text{m}$. To avoid possible damage to the SLM, we keep the intracavity power below two thirds of the damage threshold. Before the introduction of SPD, the fundamental Gaussian mode was emitted at a wavelength of 1064 nm under a pump power of more than 1.8 W from the 808-nm laser diode, and the fitted threshold pump power was 1.3 W. The pump is modulated to emit a laser for 20 ms at 10 Hz

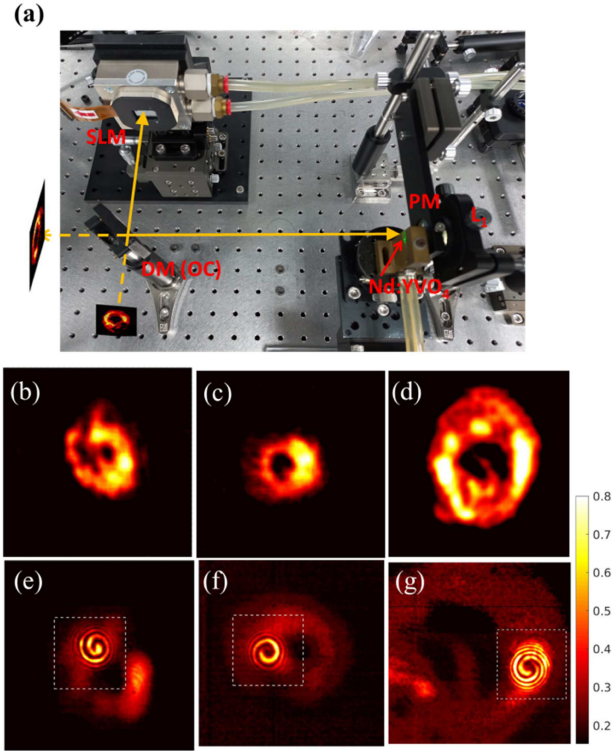


Fig. 4. (a) Photograph of the experimental setup of a laser resonator with SPDs encoded by SLM. PM is a pump mirror with high reflectivity ($>99.9\%$) at 1064 nm. DM (OC) is the dichroic mirror coated for 45° incidence with high reflection ($>99.4\%$) at 1064 nm and high transmission at 808 nm. Nd:YVO₄ is the laser gain media with double side anti-refraction coating at 1064 nm. Examples of the emitted doughnut-shaped laser beam profiles (b, c, d) taken in the region enclosed by white dashed square are shown, along with the corresponding interference fringes, indicating that the topological charges of the vortex lasers are (e) +1, (f) -1 and (g) +2. The topological charge of SPD for (b), (c) and (d) are +1, -1 and 2, respectively and the radius of SPD is $400\ \mu\text{m}$ corresponding to a scale radius of 1.704.

so that the averaged power incident on the SLM can be reduced to prevent optical damage to the SLM.

Encoding SPD along concave phase (radius of curvature is 20 cm) on SLM and maintain the cavity length of 15 cm, donut-shaped laser beams shown in Fig. 4(b)–(d) were emitted when pump was above a threshold for various topological charges and radius of SPDs. Direct signature identifying the OAM property of the lasers are shown in Fig. 5(e)–(g) respectively by the interference fringes measured from a homemade Mach–Zehnder interferometer in which the setup can be found in Fig. 2(a) in [26]. In that interferometer, the two beams divided from a single vortex laser are displaced deliberately after the beam combiner (the second beam splitter) and one of the beams is focused onto the ring region of another beam which expands freely and becomes a background field with a flat wavefront. Interference fringes were recorded by a CCD camera for further investigation. The clear spiral interference patterns in Fig. 5(e)–(g) not only quantifies the topological charge of the +1, -1 and +2 in the optical vortices, which imitate the topological charge of the SPD encoded by the SLM in the laser resonator, but also manifests the high spatial coherence of the vortex laser beam from ASB resonators [26], [32].

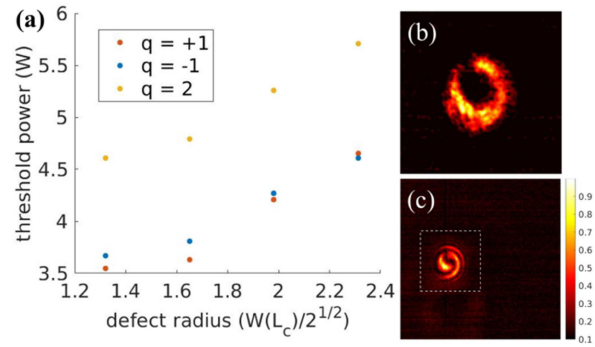


Fig. 5. (a) Threshold powers of vortices lasing in a resonator with SPDs carrying topological charges of +1 (red), -1 (blue), and +2 (yellow). The threshold powers increase with defect radii. Emission of doughnut-shaped laser beam profiles (b) carrying a topological charges of +2 shown in (c) was observed given that the topological charge of SPD is +1 and scaled radius of SPD is 1.874.

When the radius of the SPD is increased gradually, $\sigma_{0,0}^{l,l-q}$ increases, indicating that the modal coupling is stronger. However, the modal loss $\sigma_{0,0}^{l,l}$ increases; consequently, the laser threshold increases accordingly, as confirmed experimentally in Fig. 5(a). As shown in Fig. 5(a), at a comparable lasing threshold of the vortex with a topological charge of +1, a doughnut-shaped beam carrying a topological charge $q = -1$ is emitted when the topological charge of SPD was flipped from $q = +1$ to $q = -1$, which are shown in Fig. 4(e) and (f), respectively. For a defect radius greater than $440\ \mu\text{m}$ corresponding to a scale radius of 1.874, a vortex carrying a topological charge of +2 was observed while the topological charge of SPD remains +1, as shown in Fig. 5(b) and (c) for the intensity and interference pattern, although it was not stable. It is due to the cascade coherent scattering process which is discussed in next section. Encoding the SPD to carry a topological charge of $q = +2$, a vortex beam with a topological charge of +2 was generated at higher average threshold power, as shown in Fig. 4(d) for the doughnut-shaped intensity distribution and Fig. 4(g) for the phase structure of the double-spiral pattern. The capability of topological charge manipulation using a finite-sized SPD is obvious. Laser operation with a pure absorptive defect was not done in the experiment because of the limit of phase-only modulation in the SLM. The evidence can be found in a report by Kano et al. in 2012 [19].

Because the SLM has a fill factor of 0.95 for each cell $7.8\ \mu\text{m}$ in width and is placed as an array with a pitch of $8\ \mu\text{m}$, the modal coupling efficiency denoted by (3) and the modal loss given by (4) are reduced simultaneously. The formation of vortices, starting with spontaneously emitted photons distributed in a manner similar to the intensity distribution of the pump beam, becomes less desirable. The increase in the defect radius is favorable, so a particular vortex state succeeds in the competition among the supported LG_p^l modes. The scaled defect radius in the experiments, as shown in Fig. 5(a), was thus larger than the predicted value computed using (5)–(7) and illustrated in Fig. 3(a) and (d). By fitting the interference fringe with that of the coherent superposition of multiple vortices [26], observation of the vortex carrying topological charge as a multiple of the

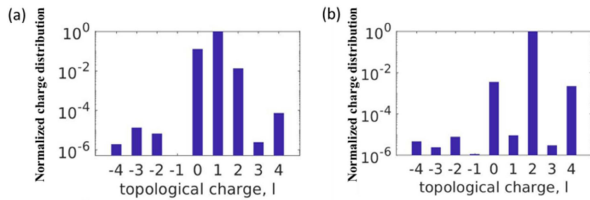


Fig. 6. (a) and (b) reveals the distribution of the fitted topological charge components of Fig. 4(b) and (d), respectively.

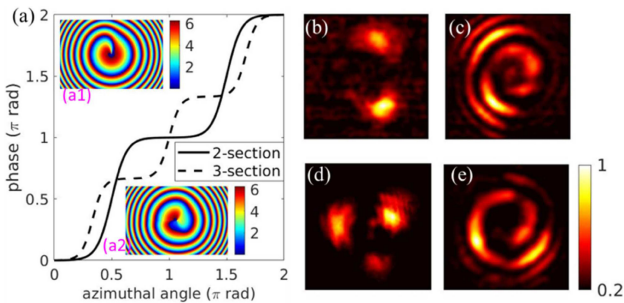


Fig. 7. (a) Deformed azimuthal phase of the SPDs forming two (solid line) and three (dashed line) plateau sections. The insets a1 and a2 reveal the phase modulation provided by the SLM. (b), (c) Recorded laser intensity distribution and interference pattern using the SLM modulation illustrated in a1. (d), (e) Recorded laser output and phase structure using three-section SLM modulation illustrated in a2. The defect radii are both $\rho_{SPD} = 1.982$ ($480 \mu\text{m}$ in real dimension) and the pump powers are both 5.29 W .

topological charges in the SPD shown in Fig. 6(a) and (b) indicates that the generation of a high-order vortex from the cascade coupling process, such as the vortex of topological charges -2 and -3 in Fig. 3(b), vortex of topological charge $+2$ and $+3$ in Fig. 3(c), and vortex of topological charge $+4$ in Fig. 3(d), is possible. However, cascade coupling seems to be unlikely in practical experiments, which can be attributed to the low coupling efficiency and a relatively high cavity loss for the high-order modes. The topological charge distribution of the vortex carrying a topological charge of $+2$ is also calculated from its interference image in Fig. 4(d). It also contains small amount of components of topological charge of 0 and $+4$, respectively. Their relative strength is 0.1% of the major component at the topological charge of $+2$. It is also obvious that the topological charge components of $+1$ and $+3$ are even smaller because their coupling to most possible spontaneous emission pattern without orbital angular momentum are impossible. Although the vortex purity of vortex laser reported in this work is not as pure as the azimuthal symmetry breaking laser cavity resonating off-axis modes [26], proper phase modulation pattern with SPDs can be designed and implemented by SLM to improve the vortex purity.

The phase modulation capability of SLM supports vortex generation with controllable topological charges by creating a combination of a finite-sized SPD and a concave mirror. It can be encoded to manipulate the intensity distribution of the vortices. By deforming the SPDs in the azimuthal direction, as illustrated in Fig. 7(a), one can concentrate the vortex intensity in the area where the phase gradient in the azimuthal direction is the least in

modulo. This behavior is similar to the amplitude–phase relation of azimuthons with zero angular velocity [34]. Experimental demonstrations of the azimuthally localized vortex laser carrying a topological charge of $+1$ are shown in Figs. 7(b) and (c), respectively, when the SLM is encoded to provide the phase modulation given by the insets a1 and a2 in Fig. 7(a). Although the intensity distributions of the vortices are concentrated at two or three spots, the phase structures revealed by interferometry verify a topological charge of $+1$.

IV. CONCLUSION

The concept of an SPD was introduced in resonator design, resulting in the generation of a topological-charge-controllable vortex laser. With a finite radius in the SPD, ladder functions for OAM can be avoided and stable laser resonance can be achieved under the balance of modal losses, intermodal coherent scatterings controlled by topological charges and radius of SPD and the modal gain manipulated by pumping configuration. Theoretical models and calculations predicted the manipulation of the topological-charge distribution of the emitted vortex laser by adjusting the defect size and selecting the topological charge of the spiral phase. These topological-charge-controllable vortex lasers were realized using a digital laser configuration. Azimuthon-like radiations were also experimentally demonstrated. This work suggests that SPDs provide a powerful approach to achieve digital control of optical vortices and can be of great use for related applications.

ACKNOWLEDGMENT

Data availability: The data that support the findings of this study are available from the corresponding authors, Y.-Y. Lin upon reasonable request. The authors declare no conflicts of interest.

REFERENCES

- [1] A. Forbes, M. de Oliveira, and M. R. Dennis, “Structured light,” *Nature Photon.*, vol. 15, pp. 253–262, 2021.
- [2] A. Forbes, “Structured light from lasers,” *Laser Photon. Rev.*, vol. 13, 2019, Art. no. 1900140.
- [3] H. Huang et al., “100 Tbit/s free-space data link enabled by three-dimensional multiplexing of orbital angular momentum, polarization, and wavelength,” *Opt. Lett.*, vol. 39, pp. 197–200, 2014.
- [4] B. Wang, J. Shi, T. Zhang, X. Xu, Y. Cao, and X. Li, “Improved lateral resolution with an annular vortex depletion beam in STED microscopy,” *Opt. Lett.*, vol. 42, pp. 4885–4888, 2017.
- [5] Y. Yang, Y.-X. Ren, M. Chen, Y. Aritac, and C. Rosales-Guzmán, “Optical trapping with structured light: A review,” *Adv. Photon.*, vol. 3, 2021, Art. no. 034001.
- [6] R. A. B. Suarez, A. A. R. Neves, and M. R. R. Gesualdi, “Optimizing optical trap stiffness for Rayleigh particles with an Airy array beam,” *J. Opt. Soc. Amer. B*, vol. 37, pp. 264–270, 2020.
- [7] R. A. B. Suarez, A. A. R. Neves, and M. R. R. Gesualdi, “Optical trapping with non-diffracting Airy beams array using a holographic optical tweezers,” *Opt. Laser Technol.*, vol. 135, 2021, Art. no. 106678.
- [8] J. Hamazaki, R. Morita, K. Chujo, Y. Kobayashi, S. Tanda, and T. Omatsu, “Optical-vortex laser ablation,” *Opt. Exp.*, vol. 18, pp. 2144–2151, 2010.
- [9] A. E. Willner, K. Pang, H. Song, K. Zou, and H. Zhou, “Orbital angular momentum of light for communications,” *Appl. Phys. Rev.*, vol. 8, 2021, Art. no. 041312.
- [10] A. M. Yao and M. J. Padgett, “Orbital angular momentum: Origins, behavior and applications,” *Adv. Opt. Photon.*, vol. 3, pp. 161–204, 2011.

- [11] R. A. B. Suarez, A. A. R. Neves, and M. R. R. Gesualdi, "Generation and characterization of an array of Airy-vortex beams," *Opt. Commun.*, vol. 458, pp. 124846, 2020.
- [12] M. Golbandi and A. Sabatyan, "Controlling and shaping topological charge by means of spiral petal-like zone plate," *Opt. Laser Technol.*, vol. 134, 2021, Art. no. 106574.
- [13] L. Marrucci et al., "Spin-to-orbital conversion of the angular momentum of light and its classical and quantum applications," *J. Opt.*, vol. 13, 2011, Art. no. 064001.
- [14] S. Katz, N. Kaplan, and I. Grossinger, "Using diffractive optical elements," *Laser Technik J.*, vol. 15, pp. 29–32, 2018.
- [15] G. Gibson et al., "Free-space information transfer using light beams carrying orbital angular momentum," *Opt. Exp.*, vol. 12, pp. 5448–5456, 2004.
- [16] T. Omatsu, K. Miyamoto, and A. J. Lee, "Wavelength-versatile optical vortex lasers," *J. Opt.*, vol. 19, 2017, Art. no. 123002.
- [17] R. Oron, Y. Danziger, N. Davidson, A. A. Friesem, and E. Hasman, "Laser mode discrimination with intra-cavity spiral phase elements," *Opt. Commun.*, vol. 169, pp. 115–121, 1999.
- [18] R. Oron, N. Davidson, A. A. Friesem, and E. Hasman, "Efficient formation of pure helical laser beams," *Opt. Commun.*, vol. 182, pp. 205–208, 2000.
- [19] A. Ito, Y. Kozawa, and S. Sato, "Generation of hollow scalar and vector beams using a spot-defect mirror," *J. Opt. Soc. Amer. A*, vol. 27, pp. 2072–2077, 2010.
- [20] K. Kano, Y. Kozawa, and S. Sato, "Generation of a purely single transverse mode vortex beam from a He-Ne laser cavity with a spot-defect mirror," *Int. J. Opt.*, vol. 2012, 2012, Art. no. 359141.
- [21] Y. F. Chen and Y. P. Lan, "Dynamics of the Laguerre Gaussian $TEM_{0,1}$ mode in a solid-state laser," *Phys. Rev. A*, vol. 63, 2001, Art. no. 063807.
- [22] D. Lin, J. M. O. Daniel, and W. A. Clarkson, "Controlling the handedness of directly excited Laguerre-Gaussian modes in a solid-state laser," *Opt. Lett.*, vol. 39, pp. 3903–3906, 2014, Art. no. 3903.
- [23] D. J. Kim and J. W. Kim, "Direct generation of an optical vortex beam in a single-frequency Nd:YVO₄ laser," *Opt. Lett.*, vol. 40, pp. 399–402, 2015.
- [24] W. R. Kerridge-Johns, J. W. T. Geberbauer, and M. J. Damzen, "Vortex laser by transforming Gaussian mode with an interferometric output coupler," *Opt. Exp.*, vol. 27, pp. 11642–11650, 2019.
- [25] D. Naidoo et al., "Controlled generation of higher-order Poincaré sphere beams from a laser," *Nature Photon.*, vol. 10, pp. 327–333, 2016.
- [26] Y.-Y. Lin, C.-C. Yeh, H.-C. Lee, S.-L. Yang, J.-H. Tu, and C.-P. Tang, "Optical vortex lasers by the coherent superposition of off-axis multiple-pass transverse modes in an azimuthal symmetry breaking laser resonator," *J. Opt.*, vol. 20, 2018, Art. no. 075203.
- [27] S. Ngcobo et al., "A digital laser for on-demand laser modes," *Nature Commun.*, vol. 4, 2013, Art. no. 2289.
- [28] C.-Y. Huang, K.-C. Chang, and S.-C. Chu, "Experimental investigation of generating laser beams of on-demand lateral field distribution from digital lasers," *Materials*, vol. 12, 2019, Art. no. 2226.
- [29] Y. Lin and Y. Lee, "Vortex laser generation with controllable topological charges in a spiral phase defect resonator," in *Proc. Frontiers in Optics + Laser Sci.*, C. Mazzali, T. (T.-C.) Poon, R. Averitt, and R. Kaindl, Eds., 2021, Paper JTU1A.9.
- [30] E. T. Whittaker, "An expression of certain known functions as generalized hypergeometric functions," *Amer. Math. Soc.*, vol. 10, no. 3, pp. 125–134, 1903.
- [31] J. Dong, K. Ueda, and P. Yang, "Multi-pulse oscillation and instabilities in microchip self-Q-switched transverse-mode laser," *Opt. Exp.*, vol. 17, pp. 16980–16993, 2009.
- [32] Y.-Y. Lin, J.-H. Tu, H.-C. Lee, S.-L. Yang, and C.-P. Tang, "Bifurcation and nonlinear dynamics in passive Q-switched optical vortex lasers," *J. Opt.*, vol. 21, 2019, Art. no. 085201.
- [33] A. Sinha and G. Barbastathis, "Resonant holography," *Opt. Lett.*, vol. 27, pp. 385–387, 2002.
- [34] A. S. Desyatnikov, A. A. Sukhorukov, and Y. S. Kivshar, "Azimuthons: Spatially modulated vortex solitons," *Phys. Rev. Lett.*, vol. 95, 2005, Art. no. 203904.